JMEPEG (2008) 17:561–565
DOI: 10.1007/s11665-007-9167-3

1059-9495/$19.00

# Mössbauer Effect Study of Room Temperature Cathodic Polarization of AISI321SS Austenitic Stainless Steel

*Oswald N.C. Uwakweh and Vinod S. Agarwala*

*(Submitted January 5, 2007; in revised form March 7, 2007)*

**Room temperature hydrogen charging by cathodic polarization of cold rolled AISI 321SS austenitic stainless steel in appropriate electrolytic medium leads to its decomposition to structural defects and a ferromagnetic α′-martensitic phase. The degree of decomposition, and hence the resulting products depends on hydrogen charging time with martensitic transformation yielding up to 14-22% martensite for charging periods of 30 and 96 h, respectively. Based on Mössbauer spectroscopy measurements, the magnetically split portion of the spectra corresponding to the α′-martensite phase was resolved in terms of one Fe-site with internal magnetic field in the range of 260-265 ± 10 kOe. Both the uncharged and retained (after hydrogen charging) austenitic phases were resolved similarly at ambient and sub-ambient cryogenic temperatures. The austenitic phase in both the uncharged and charged states remained stable from ambient down to 4.2 K, where they exhibited singlet broadening suggesting weakly ferro/antifero-magnetic ordering.**

**Keywords** AISI-321 austenitic stainless steel, cathodic hydrogen charging, martensite, Mössbauer spectroscopy

## 1. Introduction

The interaction of hydrogen with a variety of metallic materials is often of considerable interests for differing reasons (Ref 1-5). For instance, when metallic materials are exposed to hydrogen rich or hydrogen producing environments, a phenomenon described as hydrogen embrittlement can occur at levels spanning the macroscopic down to the atomic scales. One of the reasons for the interest in hydrogen materials interaction is based on its deleterious effect on the mechanical properties of these materials. In this regard high-strength steels with multi-phase structures, or the single phased stainless types are of major interest due to their versatility of use in structural applications. The single phased austenitic stainless steels including, both the stable and unstable types can be adversely affected by entry of hydrogen to a large extent as manifested by their transformation (Ref 6-9).

Stainless steels are usually employed structurally or under corrosive environments due to their abilities to resist corrosion (Ref 9-11). The AISI304SS grades are one of the austenitic stainless steels that are most widely used. However, because of its inherent property loss when used in the 450-650°C temperature range (due to the formation of complex chromium carbides along grain boundaries), a version known as AISI 321SS was developed. AISI 321SS austenitic stainless steel is in effect a Ti stabilized 304 which is used in aircraft exhausts manifolds and flanges, and also in jet engines parts because of its improved elevated temperature resistance. Despite this modification, AISI 321SS is known to suffer phase decomposition when subjected to low-cycle fatigue (Ref 12), or when subjected to compression, tension, and friction tests (Ref 13). The product of decomposition has been generally reported as a BCC martensitic phase (Ref 12, 13).

During room temperature hydrogen cathodic or gas phase charging of types AISI 304SS and AISI 305SS steels, formation of hexagonal ε-martensite phase and/or BCC α′-martensitic phase (Ref 7, 14-20) have been reported unlike in the case of high carbon Fe-C alloys (Ref 14) where only α′-martensite formed with cathodic charging. This observation was in contrast to the case of AISI-310SS steel, where it was reported that formation of ε-phase (with dissolved hydrogen) prevented the formation of α′-martensite, while reverting back to the γ-phase with aging treatments according to Okada et al. (Ref 20).

Owing to the above observations, room temperature hydrogen cathodic charging of AISI 321SS was performed under comparable conditions as reported for high carbon steel (Ref 14), and AISI 304SS and AISI 305SS (Ref 7, 15-19). The objective of this work was to investigate the phase transformation behavior of AISI-321 austenitic stainless steel in order to verify the relationship between ε and α′-martensite phases with combined x-ray diffraction (XRD) and Mössbauer spectroscopic (MS) techniques. In this study, we report the first account (to the best of our knowledge) of the room temperature hydrogen charging by cathodic polarization of AISI-321-austentic alloy in an electrolytic bath consisting of dilute acid solutions impregnated with hydrogen recombination inhibitor also referred to as poison or promoter.

## 2. Experimental

The AISI 321SS samples of this study were obtained by cutting rectangular portions measuring 2 cm × 10 cm from a

**Oswald N.C. Uwakweh**, Department of Engineering Science and Materials, College of Engineering, University of Puerto Rico—Mayagüez, 9044, Mayagüez 00681-9044, Puerto Rico; and **Vinod S. Agarwala**, Naval Air Systems Command, 48110 Shaw Road, Bldg. 2187/Suite 237, Patuxent River, MD 20670-1906. Contact e-mail: uwakweh@ece.uprm.edu.

**Table I Composition of AISI 321SS austenitic stainless steel**

| Chemical composition (Wt Pct) | | | | | | | | |
|---|---|---|---|---|---|---|---|---|
| C | Mn | Si | Cr | Ni | Ti | S | P | Fe |
| 0.08 max | 2.00 max | 1.00 max | 17.0/19.00 | 9.0/12.00 | 5 x%(C + N); max = 0.7 | 0.03 max | 0.045 | Bal |

50 μm (0.002″) thick cold rolled foil which was supplied by SHOPAID Inc., Woburn, MA 01801, USA. The composition of type AISI 321SS austenitic steel is shown in Table 1 below. Prior to the charging operations, the samples were cleaned in methanol repeatedly and then blow air dried in order to eliminate any forms of grease or contaminants on the surface.

The samples were hydrogen charged by cathodic polarization in aqueous sulfuric acid ($H_2SO_4$) electrolytic medium which was impregnated with promoters, or ''poisons'' of the type ($As_2O_5$(V)) in order to aid hydrogen ingress in the austenitic steel. The overall composition of the medium was thus 0.1 M $H_2SO_4$ + 1g/l $As_2O_5$(V). The cathodic polarization was realized by imposing constant charging current densities, which ranged from 50 to 500 mA/cm$^2$ for times varying from 1 to 96 h. The samples were suspended in the electrolyte such that only the surface for hydrogen charging was immersed in the electrolyte by means of alligator clip. This arrangement ensured that the 50 μm thick samples were hydrogen charged simultaneously from both sides of the rectangular coupons. The circuit was completed by the use of platinum counter electrode. All charging were carried out under constant current modes.

After hydrogen charging, the samples were rinsed in water followed by methanol, and then air blow dried. The samples were subsequently photographed followed by XRD and Mössbauer spectroscopy (MS) characterizations. The XRD measurements were carried out using the Rigaku-5000, with Cu $K_\alpha$ radiation at 40 kV and 35 mA. Since the diffractometer did not have low-temperature capability, there were no attempts for sub-ambient measurements. The scanning range of the XRD measurements was chosen to capture all possible diffraction peaks, which therefore necessitated measurements in the range $20° \geq 2\theta \leq 120°$.

Concerning MS, the data were collected on a WEB Research Co. spectrometer operating in the constant acceleration, transmission mode. The 1024 point raw data were folded and analyzed using WMOSS, a public domain Mössbauer spectral analysis program (based on HFD model of Rancourt (Ref 21)) available at www.webres.com. The velocity scale was calibrated using the known line positions of room temperature iron metal foil. The center of the Fe foil spectrum was used to define the zero of the velocity scale, i.e., quoted isomer shifts are relative to iron metal. Low temperature data was acquired with the sample in a Janis Research Co. liquid He cryostat. The sample was in He exchange gas where its temperature was measured with a Lakeshore silicon diode attached to the same copper block as the sample. The gamma source used was from a 25 mCi Co-57 in Rh made by Ritverc, GmbH.

Hydrogen content was not determined in this study, since the focus of the study was to determine the long-term effect of cathodic charging with the aim of determining its relative stability with respect to degradation. To this effect, the observed macroscopic distribution of the samples that occurred with cathodic polarization was used as a basis to reconcile the extent of hydrogen ingress with prolonged charging times.

**Fig. 1** Macroscopic buckling of AISI 321SS during hydrogen charging

## 3. Results and Discussion

### 3.1 Macroscopic Deformation

As can be seen in Fig. 1, macroscopic distortion of the samples occurred with hydrogen charging due to the cathodic polarization in a 0.1 M $H_2SO_4$ + 1 g/l $As_2O_5$(V) aqueous electrolyte. The conditions for the formation of macroscopic distortion was observed to correspond to continuous hydrogen charging greater than 24 h, when current density was in the range of 50-500 mA/cm$^2$. This showed that though the early stages of the decomposition of the steel being entirely microscopic, the long-term effect eventually became macroscopic distortion. The degree of macroscopic buckling (bending) observed here was also noted by Uwakweh and Genin (Ref 14) during the hydrogen charging of binary Fe-1.95C austenitic alloys at ambient temperatures. Given that hydrogen ingress was not uniform all over the exposed surface of the material, it was concluded that distribution of steep concentration gradients accompanied by formation of structural defects such as dislocations and stacking faults, etc. resulted. The combination of the formation of structural defects together with local stresses eventually culminated to the observed macroscopic buckling of the thin foil.

### 3.2 X-ray Diffraction Measurements

The room temperature XRD measurements conducted on the as-received material over the $20° \leq 2\theta \leq 120°$ range was compared to the same following cathodic hydrogen as shown charging in Fig. 2a and b, respectively. The phase decomposition accompanying the hydrogen charging was evident with the decrease in intensity of the austenitic phase peaks, and the emergence of new ones as shown in Fig. 2b.

Since the As-received material was cold rolled, therefore it was expected that texture development will occur. On this

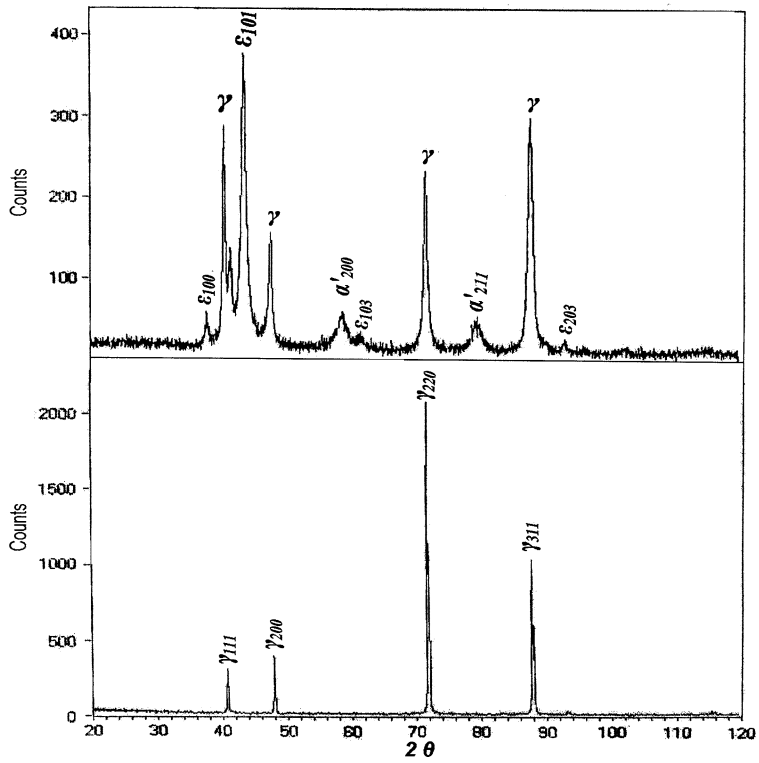


**Fig. 2** X-ray diffraction spectra for (a) As-received, and (b) 96 h of charging, after 4 days room temperature aging

consideration, the spectral peaks intensities shown in Fig. 2a were accounted for. Following cathodic polarization, the hydrogen ingress in the material provoked phase transformation which led to the formation of both hexagonal ε- and BCC α′-martensite phases as indicated in their corresponding spectral peaks in Fig. (2b) in line with Chen et al., Hoelzel et al. and, Yang and Luo, respectively (Ref 7, 16, 17). The extent of hydrogen-induced structural deformation of AISI 304SS and AISI 310SS austenitic stainless steels were neither reported by Hoelzel et al. (Ref 16) during high-temperature gas phase charging, nor by Yang and Luo (Ref 17) in the case of cathodic electrolytic charging. AISI 310SS stainless steel remained stable at 350 °C for hydrogen concentration (i.e., H/Me) range of 0.003-1.03 levels, which corresponded to gas pressure range of 3.0-7.0 GPa.

In contrast to the case of AISI 310SS steel, AISI 304SS austenitic steel decomposed to ε-martensite and eventually to α′-martensite with increasing charging pressure. According to these authors, the ε-martensite which appeared at 3.0 GPa (i.e., for H/Me = 0.56) amounted to 16 wt.% fraction of the steel. Further, squeezing AISI 304SS steel at 4.0 GPa, in the absence of hydrogen resulted in the formation of ε-martensite which accounted for 11 wt.% weight fraction, in addition to small amount of BCC α-martensite (≈ 3 wt.%).

With hydrogen charging by cathodic polarization, Yang and Luo (Ref 17) reported that ε-martensite formed within 4 min of charging, while α′-martensitic peaks were observed after 1 h charging for a 20 mA/cm$^2$ charging current density. However there was no indication of macroscopic distortion as observed in this study. Further, according to Mumtaz et al. (Ref 20), formation of α′-martensite was observed after about 15% reduction with cold rolling of AISI 304SS stainless steel. They also reported the difficulty associated with XRD resolution and subsequent quantitative analyses for deformations below 20% reduction, and stated that up to 5.7% martensite (i.e., decomposition of the austenite) was detected at 20% reduction in thickness as deduced from magnetic measurements. Interestingly, they reported about a maximum of 65% (martensite) transformation of the austenitic phase for a 55% reduction in thickness, without mention of ε-martensite. In sum, it appears therefore that the product of phase decomposition in these steels depended strongly on the process leading to their deformation. It is possible that thickness reduction by rolling operation may be transforming the austenitic phase directly to the α′-martensitic phase without going through an intermediate stage of ε-martensite. Alternatively, it is possible that the volume of interacting dislocations might have made it impossible or difficult to detect the intermediate ε-phase.

### 3.3 Mössbauer Spectroscopy (MS) Studies

The Mössbauer spectra recorded at room and cryogenic temperatures for the AISI 321SS steel in the as-received and charged states are shown in Fig. 3(a-e) respectively. As shown in Fig. 3a, the as-received material remained entirely austenitic, i.e., without magnetic transition which should have been reflected by the formation of magnetically split six peaks, from room temperature down to 4.2 K. The spectra were resolved in terms of two Fe sites having quadrupole splits of 0.08 and 0.42 mm/s respectively with corresponding relative abundances of 64 and 36% respectively. The spectral broadening observed at 4.2 K was satisfactorily fitted by using internal fields of 0.16 mm/s (23.52 kOe) and 0.31 mm/s (45.57 kOe) with relative abundances of 56% and 44%, respectively.

Figure 3c shows the spectrum of the 30 h hydrogen charged sample which together with its magnetically split peaks

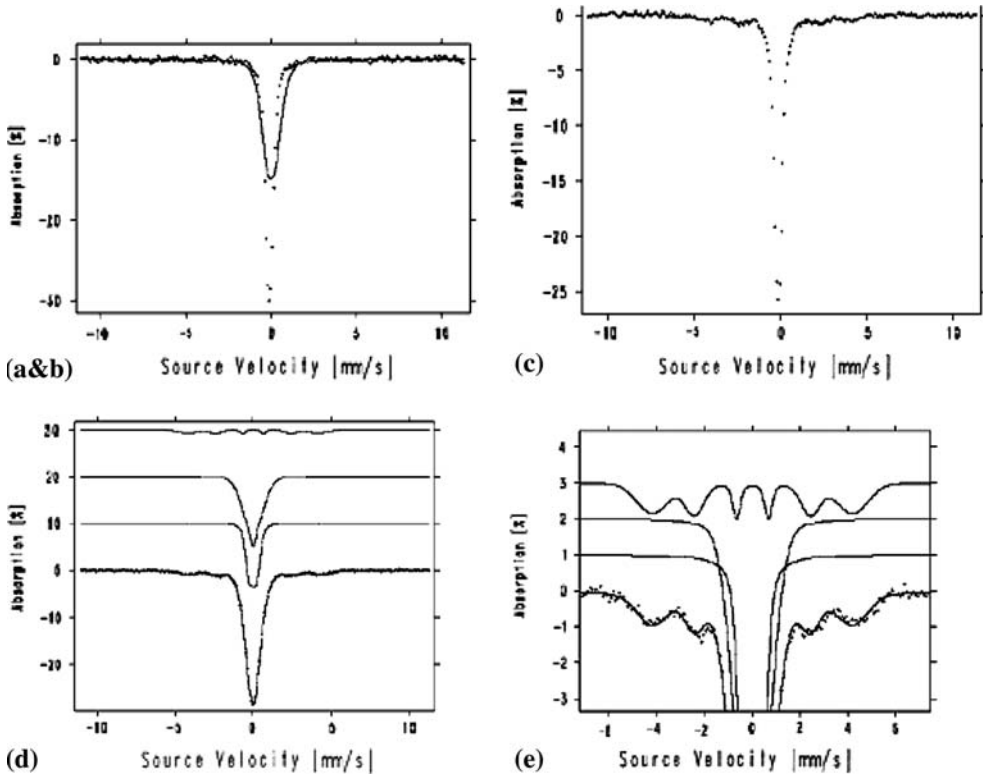


**Fig. 3** (a-e): Mössbauer spectra of As-received AISI 321SS at (a) 4.2 K (fitted) and (b) 298 K unfitted (overlaid). (c): Room temperature spectrum after hydrogen cathodic charging for 30 h showing ferromagnetic sextet peaks, and retained austenite singlet. (d): Spectral fitting of (c) at 4.2 K. (e): Enlarged portion of (d) showing the three Fe-sites

flanking the central paramagnetic retained austenite peaks as recorded at 4.2 K. Accordingly, the spectrum was fitted with three Fe sites attributed correspondingly to two paramagnetic and a ferromagnetic one. At ambient, the paramagnetic site with a quadrupole splitting of 0.42 mm/s had its relative abundance of 36% reduced to 21% in the charged state while the quadrupole splitting increased to 0.70 mm/s. On the other hand, at 4.2 K, the quadrupole splits of the two sites were 0.16 and 0.42 mm/s with corresponding relative abundances of 40% and 45%, respectively. We attributed this change to possible weakly ferro-/antiferromagnetic ordering. Since we were not able to measure the spectra at lower temperatures, say, at 1.2 K together with external magnetic fields, we could not categorically confirm the type of order that was responsible for the broadening. As to be expected, the magnetically split site is attributed to the formed martensite, and accounted for 18% in relative abundance, having corresponding internal fields of 242.55 kOe at room temperature, while 258.72 kOe at 4.2 K.

In fitting the spectra, the paramagnetic portion was not considered as a random solid solution having varying Fe symmetries with respect to its neighbor configuration. Even though AISI 321SS stainless steel has mainly Cr, Ni, Mn, and Ti atoms in the substitutional positions, the overall width of the singlet peak both in the as-received and hydrogen charged forms did not warrant the use of more than two Fe sites with differing quadrupole splitting at the Fe site during the spectral fitting. Further, the relative distributions accounting for the broad peak did not appear to be a factor associated with phase transformation from the consideration of the spectral features observed in the uncharged as-received and charged samples.

Our consideration was in contrast to that of Cook (Ref 22) who analyzed Mössbauer spectra of strain-induced martensitic transformation of AISI 316SS based on the distribution of quadrupole splitting around Fe atom of the austenitic phase, and magnetic field distribution for the transformed martensite daughter phase. While he reported about 30% decomposition of austenite to martensite due to the strain accompanying the brushing operation, the 251-285 KOe reported for Fe atoms with three and two nearest neighbor solute atoms appeared in agreement with our result on the hydrogen-induced martensitic transformation of AISI 321SS. It should be noted that his values were based on conversion electron Mössbauer spectroscopic (CEMS) measurements which implied that the probing was within 3000 Å of the material's surface, in contrast to our case where transmission measurements entailed probing the entire material volume exposed to the $\gamma$-ray.

In Fig. 3c and d, the spectra of the charged material measured at ambient and 4.2 K are shown to include both the ferromagnetic sextets associated with the martensitic phase, and the paramagnetic retained austenite. Figure 3d on the other hand showed the magnified portion of the fitted spectrum at 4.2 K with the ferromagnetic and paramagnetic sites. The observed changes in the Mössbauer parameters observed in the spectra of the as-received and charged samples measured at ambient and 4.2 K can be attributed as alluded earlier to a possible weakly ferro-/antiferromagnetic transition starting at 4.2 K. It is possible that in-field measurements would yield additional information in future studies. From these considerations, one could unambiguously attribute the ferromagnetic peaks of the charged sample to unique Fe sites in $\alpha'$-martensite

phase, and not to the ε-martensite which is either devoid of unique Fe sites/ Fe constituent, or mere structural defect observed in XRD measurements.

## 4. Conclusion

The following conclusions could be drawn from the following studies:

1. Cathodic charging of AISI 321SS austenitic stainless steel in aqueous medium impregnated with hydrogen recombination inhibitor agents or poison (0.1 M $H_2SO_4$ + 1g/l $As_2O_5$(V)) led to both macroscopic and microscopic structural phase decomposition which gave rise to the formation of ferromagnetic α′-martensite.
2. Macroscopic buckling was attributed to the inhomogeneous distribution of hydrogen accompanying the cathodic polarization due to the distribution of hydrogen concentration gradients from the immediate sub-surface down to the material interior.
3. From XRD measurements, evidence of peaks attributed to hexagonal ε-martensitic phase were observed, while not corroborated with Mössbauer Spectroscopy (MS) unlike the ferromagnetic α′-martensitic phase.
4. The martensitic phase (accounting for 14-22%) was ferromagnetic with internal magnetic field in the range of 260-265 ± 10 kOe. In the as-received form, AISI 321SS did not transform martensitically above 4.2 K, but showed a weakly ferro-/antiferromagnetic ordering at 4.2 K.
5. The retained γ-austenitic phase after hydrogen charging via cathodic polarization remained stable down to 4.2 K from ambient, showing similarly as in the uncharged state slight evidence of weak ferro-/antiferromagnetic ordering.


### Acknowledgments

The authors would like to thank Mr. Kowalik and Charles Lei for helping in the XRD measurements in Naval Air Systems Command, Patuxent River, MD. In addition, Oswald N.C. Uwakweh wishes to acknowledge the support of Dr. Yapa Rajapakse, the program manager of ONR-grant No. N000140310540.


### References


1. P. Balnchard and A.R. Troiano, La fragilisation des metaux par l'hydrogene etc (Hydrogen Embrittlement of Metals), *Memoires Scientifiques de la Revue de Metallurgie*, 1960, **57**(6), p 409–422
2. A.R. Troyano, Embrittlement by Hydrogen and Other Interstitials, *Metal Prog*, 1960, **77**(2), p 112–117
3. R.A. Oriani, Hydrogen Embrittlement of Steels, *Annual Rev. Mater. Sci.*, 1978, **8**, p 327–357
4. H.K. Birnbaum, *Environment—Sensitive Fracture of Engineering Materials*, Z.A. Forouis, Ed., (Warrendale, PA), The American Institute of Mining, Metallurgical, and Petroleum Engineers, 1979, p 326
5. J.P. Hirth, Effects of Hydrogen on the Properties of Iron and Steel, *Metall. Trans.A*, 1980, **11A**(6), p 861–890
6. J. Burke, M.L. Mehta, and R. Narayan, Hydrogen Embrittlement of Type 304L Austenitic Stainless Steel, *International Congress on Hydrogen in Metals*, (Paris), (1972), 149–158
7. S. Chen, M. Gao, and R.P. Wei, Hydride Formation and Decomposition in Electrolytically Charged Metastable Austenitic Stainless Steels, *Metall. Mater Trans A.*, 1996, **27A**(1), p 29–40
8. N. Narita, C.J. Altstetter, and H.K. Birnbaum, Hydrogen-Related Phase Transformation in Austenitic Stainless Steels, *Metall. Trans. A*, 1982, **13A**(8), p 1355–1365
9. D.A. Vaughan, D.I. Phalen, C.L. Peterson, and W.K. Boyd, Relationship Between Hydrogen Pickup and Susceptible Paths in Stress Corrosion Cracking of Type 304 Stainless Steel, *Corrosion*, 1963, **19**(9), p 315t–326t
10. Y.M. Liou, S.Y. Chiu, C.L. Lee, and H.C. Shih, Electrochemical Pitting Behavior of Type 321 Stainless Steel in Sulfide-Containing Chloride Solutions, *J. Appl. Electrochem.*, 1999, **29**(12), p 1377–1381
11. H.J. Basler and D. Eiffer, *Low-Cycle Fatigue and Elasto-Plastic Behavior of Materials*, K.T. Rie and P.D. Portella, Ed., (Amsterdam) Elsevier, 1998
12. M. Grosse, D. Kalkhof, L. Keller, and N. Schell, Influence Parameters of Martensitic Transformation During Low Cycle Fatigue for Steel AISI 321, *Physica B*, 2004, **350**(1–3), p 102–106
13. M. Ridlova, L. Hyspecka, F. Wenger, P. Ponthiaux, J. Galland, and P. Kubecka, Strain-Induced Martensitic Transformation in Type 321 Stainless Steel, *J. Phys. IV France*, 2003, **112**(1), p 429–432
14. O.N.C. Uwakweh and J.-M.R. Genin, Morphology and Aging of the Martensite Induced by Cathodic Hydrogen Charging of High-Carbon Austenitic Steels, *Metall. Trans. A*, 1991, **22A**, p 1979–1991
15. S. Chen, M. Gao, and R.P. Wei, Phase Transformation and Cracking During Aging of an Electrolytically Charged Fe18Cr12Ni Alloy at Room Temperature, *Scripta Metall. Mater.*, 1993, **28**(4), p 471–476
16. M. Hoelzel, S.A. Danilkin, H. Ehrenberg, D.M. Toebbens, T.J. Udovic, H. Fuess, and H. Wipf, Effects of High Pressure Charging on the Structure of Austenitic Stainless Steels, *Mater. Sci. Eng. A*, 2004, **A384**(1–2), p 255–261
17. Q. Yang and J.L. Luo, Martensite Transformation and Surface Cracking of Hydrogen Charged and Degassed Type 304 Stainless Steel, *Mater. Sci. Eng. A*, 2000, **A288**(1), p 75–83
18. S.L. Zevin and Z. Melamed, X-ray Diffraction by Cathodically Charged Austenitic Stainless Steel, *J. Appl. Cryst.*, 1985, **18**(5), p 267–271
19. V.G. Gavriljuk, H. Hänninen, A.S. Tereshchenko, and K. Ullakko, Effects of Nitrogen on Hydrogen-Induced Phase Transformations in Stable Austenitic Steel, *Scripta Metall. Mater.*, 1993, **28**(2), p 247–252
20. K. Mumtaz, S. Takahashi, J. Echigoya, Y. Kamada, L.F. Zhang, H. Kikuchi, K. Ara, and M. Sato, Magnetic Measurements of Martensitic Transformation in Austenitic Stainless Steel After Room Temperature Rolling, *J. Mater. Sci.*, 2004, **39**(1), p 85–97
21. D.G. Rancourt and J.Y. Ping, Voigt-Based Methods for Arbitrary-Shape Static Hyperfine Parameter Distributions in Mössbauer Spectroscopy, *Nucl. Instr. Meth. Phys. Res. Sect. B*, 1991, **B58**(1), p 85–97
22. D.C. Cook, Strain Induced Martensite Formation in Stainless Steel, *Metall. Trans. A.*, 1987, **18A**, p 201–210